IET Power Electronics

Research Article

IET Journals
The Institution of Engineering and Technology

Design and implementation of type-II and type-III controller for DC–DC switched-mode boost converter by using *K*-factor approach and optimisation techniques

ISSN 1755-4535
Received on 24th February 2015
Revised on 16th October 2015
Accepted on 22nd October 2015
doi: 10.1049/iet-pel.2015.0144
www.ietdl.org

Arnab Ghosh ✉, *Subrata Banerjee, Mrinal Kanti Sarkar, Priyanka Dutta*

Department of Electrical Engineering, National Institute of Technology, Durgapur 713209, India
✉ *E-mail: aghosh.ee@gmail.com*

Abstract: DC–DC power supplies are playing significant role in different domains of engineering applications. Some converters such as boost, buck-boost, and fly-back have a right-half-plane zero (non-minimum phase system), hence it is difficult for the PID controller to exhibit good performance with load, line variations and parametric uncertainty. In this proposed work, design and implementation of type controllers have been performed by using *k*-factor approach and two different optimisation techniques (gravitational search algorithm and particle swarm optimisation) for obtaining better stability and performance for a closed loop DC–DC Switched mode boost converter. The closed loop control system has been implemented in real time dSPACE platform. The comparative closed-loop performances of a boost converter with classical, optimised PID and optimised type II/type III controllers have been produced. Simulations and experimental results are provided to demonstrate the effectiveness of optimised controllers for the proposed converter. Design and implementation of optimised type controller for switch mode converters has not been reported earlier in any literature.

1 Introduction

The DC–DC switched mode power supply (SMPS) is well known for its extensive applications from couple of watts to several megawatts in any engineering field. The most widely recognised and vital applications are in electronic goods and gadgets, battery chargers, DC servo drives, electric transportation system, medical instruments, defence equipments, process control plant and robot automated factories, high-voltage DC transmission system, interconnection of photovoltaic and wind-electric systems to the utility grid etc. [1].

In the course of the most recent decades, the improvements of the DC–DC SMPS are taken place by introducing of different kinds of controllers [2] to achieve the fast dynamic responses as well as better reliability and power density. Generally the performance of DC–DC switching converter can be characterised into two classes such as transient and steady-state response. The transient performance of converter is mostly carried on by the control strategies, that is, nature of the controllers [3]. On the other hand, the steady-state response is mainly maintained by the converter-topology, structural configuration of energy storage elements and operating frequency of the power supplies [3]. There are different traditional (classical) controllers (such as PI, PID, lead, lag etc.) have been developed over the years to ensure desired converter performance for the particular conditions. Some converters such as boost, buck-boost, fly-back etc. have a problem of non-minimum phase (initial undershoot) due to the presence of a right-half-plane (RHP) zero in their plant transfer function [4, 5], hence it is troublesome for PID controller to show the good performance with line, load variations and parametric uncertainty. For this reason type-controllers [6–11] are best suited. In the proposed work, the design of Type controllers have been aimed by using '*k*-factor' approach and then controller parameters have to be optimised further by using different optimisation techniques for obtaining better stability and performance for a DC–DC switched mode boost converter.

The optimal controllers are based on several mechanism such as behaviour and characteristics of biological, molecular, swarm of insects, neurobiological systems etc. There is no particular algorithm to accomplish the best solution for all optimisation problems. Some algorithms may give better solution for some specific problems than others. In this work, particle swarm optimisation (PSO) [12–15] and gravitational search algorithm (GSA) [16, 17] are cast off for designing the optimal controllers. These algorithms are simple to understand, easy to implement and gives the optimum controller performance. The DC–DC SMPS are essential to deliver regulated output voltage with fast dynamical response, low overshoot, minimal steady-state output error, and low sensitivity to the noise. Some recent literatures have been reported on PSO, GSA and other algorithms based optimised PI, PID controllers [18–35] for improving the performance of the converters and other systems. However, optimised type-II/III controllers have not been reported for DC–DC converters in any literature. This proposed optimal type II/III controllers are the best suited for those converter which have the problem of non-minimum phase such as boost converter. All the requirements have to be satisfied both through the correct design of the circuit parameters, selection of components and mostly by the implementation of appropriate control methodologies.

The proposed boost converter is designed and fabricated in laboratory scale and the specifications are shown in Table 1. The design procedure is strictly followed to obtain the required voltage and power output of the converter. The implementation of the overall closed loop system is performed by utilising dSPACE real time controller. The schematic diagram of the overall control system which is being implemented is shown in Fig. 1. From the Fig. 1, it has been noted that the proposed boost converter is operated in voltage mode control where the converter output voltage is sensed by LV-25P (LEM make Hall effect voltage transducer). Then the voltage signal from sensor is appropriately conditioned (filtered and scaled) before feeding to the ADC port of dSPACE controller. The overall control system has been implemented in real time platform by using Simulink module. The conditioned digital voltage output from ADC is compared with a reference voltage; an error signal is generated and is passed through the proposed optimised type controllers which in turn

Table 1 Parameters of boost converter

Circuit components	Values
input voltage V_{in}	5 V
output voltage V_o	12 V
inductance L	250 μH
output capacitance C	1056 μF
inductor resistance r_l	10 mΩ
ESR of capacitor r_c	30 mΩ
load resistance R_{load}	25 Ω
switching period T_s	50 μs
height of triangular wave V_p	10

generates the modulating signal. This control signal is then compared with the high frequency triangular waveform to produce PWM signal. This PWM output from dSPACE is passed through DAC, Optoisolator and Astable mutivibrator circuit before inputting to the gate of MOSFET switch of boost converter.

2 Modelling of switch-mode boost converter

A mathematical model of the boost converter can be constructed using the well-known state space averaging technique [1, 2, 36–42], assuming the parameters have their nominal values. This technique practically links each other with the linear and time-invariant mathematical models which describe the converter in correspondence to its conduction configurations. Its validity is ensured if the basic frequency of the PWM waveform, which controls the converter, is much higher than the natural frequencies of the converter [43]. The mathematical model obtained by the above technique is still non-linear. From this model, a linear- and time-invariant small-signal model can be derived by means of linearisation around a well-defined operating point.

The switching converters are driven by the external switching pulses, hence, different voltage and current equations can be established among the state variables (inductor currents and capacitor voltages), and the converter can be transformed into state-space models. Then the transfer function of the boost converter can be found out by using state-space averaging method and is shown in this following Section 2.1. The injected-absorbed-current (IAC) method [38] is another concept of modelling, is derived from the state-space averaging technique, and is discussed in Section 2.2.

2.1 State-space averaging model for boost converter

State-space averaging is an approximation technique that approximates the switching converter as a continuous linear system. State-space averaging requires that the effective output filter corner frequency, f_{cor}, to be much smaller than the switching frequency, f_s to minimise the output ripple. The goal of the following analysis is to obtain a small signal transfer function $\tilde{v}_o(s)/\tilde{d}(s)$, where $\tilde{v}_o$ and $\tilde{d}$ are small perturbations in the output voltage v_o and duty ratio d. When the converter operates in continuous-conduction mode, there are two circuit states: one state corresponds to when the switch is on (Fig. 2*a*) and the other to when the switch is off (Fig. 2*b*). In the equivalent circuit the elements are defined as follows: v_{in}, v_o, L, C, r_l, r_c, R_{load} are input voltage, output voltage, inductance, output capacitance, inductor resistance, esr of capacitor, and load resistance, respectively.

The lowercase letters are used to represent the variables which include the steady-state *dc* value plus a small *ac* perturbation. The small ac perturbations and the dc steady-state quantities are represented by '~' and uppercase letter respectively.

$$i_L = I_L + \tilde{i}_L,\ v_c = V_c + \tilde{v}_c,$$
$$v_{in} = V_{in} + \tilde{v}_{in},\ v_o = V_o + \tilde{v}_o,\ d = D + \tilde{d} \quad (10)$$

State equations of switch on condition (Fig. 2*a*)	State equations of switch off condition (Fig. 2*b*)	Averaging state equations over a switching cycle
$L\frac{di_L}{dt} = v_{in} - r_l i_L$ (1)	$L\frac{di_L}{dt} = v_{in} - r_l i_L - v_o$ (4)	$L\frac{di_L}{dt} = v_{in} - r_l i_L - (1-d)v_o$ (7)
$C\frac{dv_c}{dt} = -\frac{1}{R_{load}+r_c}v_c$ (2)	$C\frac{dv_c}{dt} = \frac{R_{load}}{R_{load}+r_c}i_L - \frac{1}{R_{load}+r_c}v_c$ (5)	$C\frac{dv_c}{dt} = \frac{(1-d)R_{load}}{R_{load}+r_c}i_L - \frac{1}{R_{load}+r_c}v_c$ (8)
$v_o = \frac{R_{load}}{R_{load}+r_c}v_c$ (3)	$v_o = \frac{R_{load}\times r_c}{R_{load}+r_c}i_L + \frac{R_{load}}{R_{load}+r_c}v_c$ (6)	$v_o = \frac{(1-d)R_{load}\times r_c}{R_{load}+r_c}i_L + \frac{R_{load}}{R_{load}+r_c}v_c$ (9)

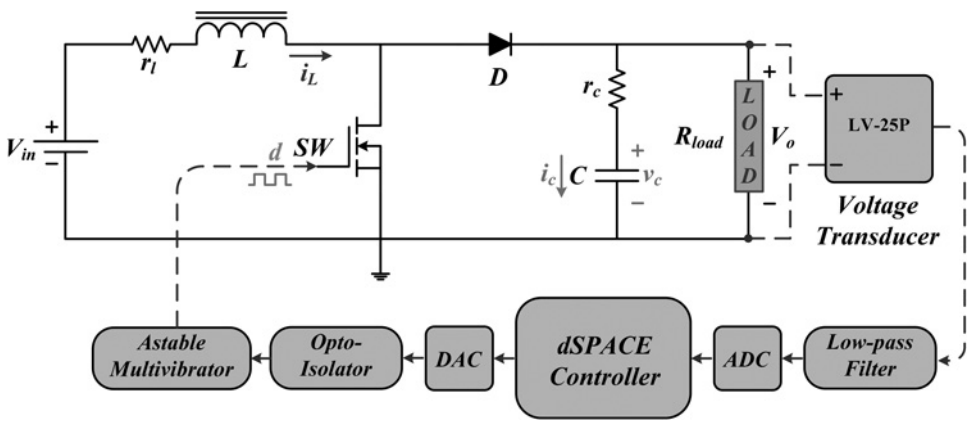

Fig. 1 *Schematic diagram of closed-loop operation for boost converter*

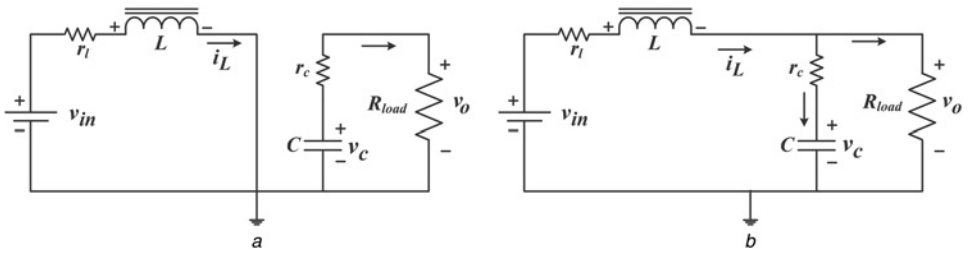

Fig. 2 *Equivalent circuit of a boost converter*

a Switch (*SW*) on
b Switch (*SW*) off instant

From (7), (8) and (9)

$$L\frac{\mathrm{d}(I_L+\tilde{i}_L)}{\mathrm{d}t}=(V_{\mathrm{in}}+\tilde{v}_{\mathrm{in}})-r_l(I_L+\tilde{i}_L)-(1-D-\tilde{d})(V_{\mathrm{o}}+\tilde{v}_{\mathrm{o}}) \quad (11)$$

$$C\frac{\mathrm{d}(V_{\mathrm{c}}+\tilde{v}_{\mathrm{c}})}{\mathrm{d}t}=\frac{(1-D-\tilde{d})R_{\mathrm{load}}}{R_{\mathrm{load}}+r_{\mathrm{c}}}\times(I_L+\tilde{i}_L)-\frac{1}{R_{\mathrm{load}}+r_{\mathrm{c}}}(V_{\mathrm{c}}+\tilde{v}_{\mathrm{c}}) \quad (12)$$

$$(V_{\mathrm{o}}+\tilde{v}_{\mathrm{o}})=\frac{(1-D-\tilde{d})R_{\mathrm{load}}\times r_{\mathrm{c}}}{R_{\mathrm{load}}+r_{\mathrm{c}}}\times(I_L+\tilde{i}_L)+\frac{R_{\mathrm{load}}}{R_{\mathrm{load}}+r_{\mathrm{c}}}(V_{\mathrm{c}}+\tilde{v}_{\mathrm{c}}) \quad (13)$$

Only considering ac quantities, the equations may be rewritten as follows (neglecting the second order ac quantities)

$$L\frac{\mathrm{d}\tilde{i}_L}{\mathrm{d}t}=\tilde{v}_{\mathrm{in}}-r_l\tilde{i}_L-(1-D)\tilde{v}_{\mathrm{o}}+V_{\mathrm{o}}\tilde{d} \quad (14)$$

$$C\frac{\mathrm{d}\tilde{v}_{\mathrm{c}}}{\mathrm{d}t}=\frac{(1-D)R_{\mathrm{load}}}{R_{\mathrm{load}}+r_{\mathrm{c}}}\tilde{i}_L-\frac{R_{\mathrm{load}}I_L}{R_{\mathrm{load}}+r_{\mathrm{c}}}\tilde{d}-\frac{1}{R_{\mathrm{load}}+r_{\mathrm{c}}}\tilde{v}_{\mathrm{c}} \quad (15)$$

$$\tilde{v}_{\mathrm{o}}=\frac{(1-D)R_{\mathrm{load}}\times r_{\mathrm{c}}}{R_{\mathrm{load}}+r_{\mathrm{c}}}\tilde{i}_L-\frac{R_{\mathrm{load}}\times r_{\mathrm{c}}I_L}{R_{\mathrm{load}}+r_{\mathrm{c}}}\tilde{d}+\frac{R_{\mathrm{load}}}{R_{\mathrm{load}}+r_{\mathrm{c}}}\tilde{v}_{\mathrm{c}} \quad (16)$$

Taking Laplace transform of (14), (15) and (16) and rearranging

$$(sL+r_l)\tilde{i}_L(s)+(1-D)\tilde{v}_{\mathrm{o}}(s)=V_{\mathrm{o}}\tilde{d}(s)+\hat{v}_{\mathrm{in}}(s) \quad (17)$$

$$\frac{(1-D)R_{\mathrm{load}}}{R_{\mathrm{load}}+r_{\mathrm{c}}}\tilde{i}_L(s)-\left(sC+\frac{1}{R_{\mathrm{load}}+r_{\mathrm{c}}}\right)\tilde{v}_{\mathrm{c}}(s)=\frac{R_{\mathrm{load}}I_L}{R_{\mathrm{load}}+r_{\mathrm{c}}}\tilde{d}(s) \quad (18)$$

$$\frac{(1-D)R_{\mathrm{load}}\times r_{\mathrm{c}}}{R_{\mathrm{load}}+r_{\mathrm{c}}}\tilde{i}_L(s)+\frac{R_{\mathrm{load}}}{R_{\mathrm{load}}+r_{\mathrm{c}}}\tilde{v}_{\mathrm{c}}(s)-\tilde{v}_{\mathrm{o}}(s)=\frac{R_{\mathrm{load}}\times r_{\mathrm{c}}I_L}{R_{\mathrm{load}}+r_{\mathrm{c}}}\tilde{d}(s) \quad (19)$$

Finally the matrix of small signal modelling has been developed from (17), (18) and (19) and the desired transfer function $T_{p\_\mathrm{boost}}(s)$ can be obtained as follows (see (20))

The transfer function of the proposed boost converter is

$$T_{P\_\mathrm{Boost}}(s)=\frac{-0.00569s^2-0.02559s+4.983\times10^6}{s^2+825.3s+542410} \quad (21)$$

From (20) and (21), it can be noted that a RHP zero has presented in the transfer function of the boost-converter plant.

2.2 IAC method

The IAC method [38] gives a more accurate transfer function for modelling of boost converters, which does not always lead to RHP zero (and the consequent step-response undershoot). The transfer function (from state-space averaging model) of the proposed boost converter (shown in Fig. 1) with neglecting the ESR of inductor and capacitor is shown in (22) by using IAC method

$$T_{P\_\mathrm{Boost}}(s)=\frac{\tilde{v}_0(s)}{\tilde{d}(s)}=\frac{V_{\mathrm{in}}/V_P(1-D)^2\left[1-s\left\{(1/1-D)^2L/R_{\mathrm{load}}+DT_s/2-T_{\mathrm{s}}\right\}\right]}{1+s\left\{(1/1-D)^2L/R_{\mathrm{load}}+T_{\mathrm{s}}/2\right\}+s^2(1/1-D)^2LC} \quad (22)$$

where, T_{s} is the switching period and V_P is the height of the triangular wave.

From (22), it can be seen that the RHP zero can sift to a LHP zero if the switching frequency (f_{s}) is low enough. The operating range of the switching frequency for this approach is [38]

$$\frac{2L}{R_{\mathrm{load}}D(1-D)^2}>T_{\mathrm{s}}>\frac{2L}{R_{\mathrm{load}}(2-D)(1-D)^2} \quad (23)$$

The upper limit ensures the continuous conduction mode while the lower limit keeps the zero in LHP. Unlike the IAC model, the state-space averaged model does not include a T_{s} term, and therefore does not predict this regime of stable operation. As the frequency approaches infinity or T_{s} approaches zero, the state-space averaging model and the IAC models converge to the same model [38].

The control to output transfer function (small signal model) of the proposed boost converter (neglecting ESR values) by using IAC method is

$$T_{p\_\mathrm{boost\_IAC}}(s)=\frac{208.3333(s+9091)}{s^2+132.6s+9.47\times10^5} \quad (24)$$

3 Description and design of type controllers

The designs of controllers will play a key role for maintaining good dynamic performances and regulation of a power supply. In this work 'classical type-II/III' controllers have been used for keeping overall closed loop stability and good dynamic response of the proposed boost converter.

$$T_{P\_\mathrm{Boost}}(s)=\frac{\tilde{v}_0(s)}{\tilde{d}(s)}=\frac{V_{\mathrm{in}}}{(1-D)^2}\frac{(1+sr_{\mathrm{c}}C)\left[1-sL/\left\{(1-D)^2(R_{\mathrm{load}}-r_l)\right\}\right]}{\left[1+sR_{\mathrm{load}}\left\{r_lC(R_{\mathrm{load}}+r_{\mathrm{c}})+L\right\}/\left\{(R_{\mathrm{load}}+r_{\mathrm{c}})\left[r_l+(1-D)^2R_{\mathrm{load}}\right]\right\}+s^2LCR_{\mathrm{load}}/r_l+(1-D)^2R_{\mathrm{load}}\right]} \quad (20)$$

3.1 Type-II controller design

The 'type-II' controller is one kind of lead type controller with a pole at origin. Hence, this controller provides maximum 90° phase boost with zero steady state error. Even though boost converter having non-minimum phase problem, it exhibits a better closed loop performance with a cascaded type-II controller. With proper tuning of this controller the converter may perform faster response, with minimal overshoots and zero steady-state error [11].

3.1.1 Mathematical approach: Type-II controller is a pair of pole-zero combination with a pole at origin. The expression of controller transfer function is

$$T_c(s) = \frac{(1 + s/\omega_z)}{(s/\omega_{po})(1 + s/\omega_p)} \tag{25}$$

where, ω_p and ω_z are respective pole and zero frequency of type-II controller.

The magnitude of such transfer function is found by replacing s by $j\omega$.

$$|T_c(j\omega)| = \frac{|1 + j\omega/\omega_z|}{|j\omega/\omega_{po}||1 + j\omega/\omega_p|} = \frac{\sqrt{1 + (\omega/\omega_z)^2}}{(\omega/\omega_{po})\sqrt{1 + (\omega/\omega_p)^2}} \tag{26}$$

The argument is written as

$$\arg T_c(j\omega) = \tan^{-1}\left(\frac{\omega}{\omega_z}\right) - \tan^{-1}\left(\frac{\omega}{\omega_p}\right) - \frac{\pi}{2} \tag{27}$$

The frequency domain response of type-II controller is plotted in Fig. 3*a*. Here the combined action of the pole, zero creates a localised phase boost (68°) at a certain frequency. The frequency where the maximum phase boost will be occurred can be obtained by taking derivate of (27).

$$\frac{d}{df}(\arg T_c(j\omega)) = \frac{d}{df}\left(\tan^{-1}\left(\frac{f}{f_z}\right) - \tan^{-1}\left(\frac{f}{f_p}\right) - \frac{\pi}{2}\right) = \frac{1}{f_z(f^2/f_z^2 + 1)} - \frac{1}{f_p\left(f^2/f_p^2 + 1\right)} = 0 \tag{28}$$

By solving (28), the maximum phase boost is obtained at the geometric means of the pole and zero frequencies, $f_{max} = \sqrt{f_p f_z}$. Generally this geometric mean frequency is considered as crossover frequency (f_c) of the controller.

3.1.2 Derivation of 'k' in type-II controller: The 'k' is defined as the ratio of the pole frequency to the zero frequency in type-II controller. These pole/zero combinations provide an adjustable phase boost from 0° to 90° at the crossover frequency. The relation between 'k' and the phase boost provided by the controller is given by (29) [11]

$$k = \tan\left(\frac{\text{phase boost}}{2} + \frac{\pi}{4}\right) \tag{29}$$

As $k = f_p/f_z$, the location of pole frequency will be

$$f_p = k.f_c = \tan\left(\frac{\text{phase boost}}{2} + \frac{\pi}{4}\right) f_c \tag{30}$$

and the zero frequency will be derived from

$$f_z = \frac{f_c}{k} = \frac{f_c}{\tan(\text{phase boost}/2 + \pi/4)} \tag{31}$$

Assuming crossover frequency (supposed to be less than the switching frequency) and phase boost, the exact locations of pole/zero can easily be found from (30) and (31).

3.1.3 Mid-band gain adjustment for the controller: A type-II controller is simply combination of single pole/zero pair with an origin pole. Controller has been described in (25) and may be described as follows

$$T_c(s) = \frac{s}{\omega_z}\frac{(\omega_z/s + 1)}{s/\omega_{po}\left(1 + s/\omega_p\right)} = \frac{\omega_{po}}{\omega_z}\frac{1 + \omega_z/s}{1 + s/\omega_p} = G_{o\_II}\frac{1 + \omega_z/s}{1 + s/\omega_p} \tag{32}$$

In the above expression, the term G_{o_II} is called the mid-band gain and G_{o_II} is equal to ω_{po}/ω_z. As ω_z is fixed by the amount of needed phase boost, ω_{po} will be placed depending on the desired gain/attenuation at crossover frequency.

3.1.4 Design example of type-II controller: Let us assume a boost converter that has a gain deficit of −18 dB at a 1 kHz (selected crossover frequency (f_c)). The necessary phase boost is

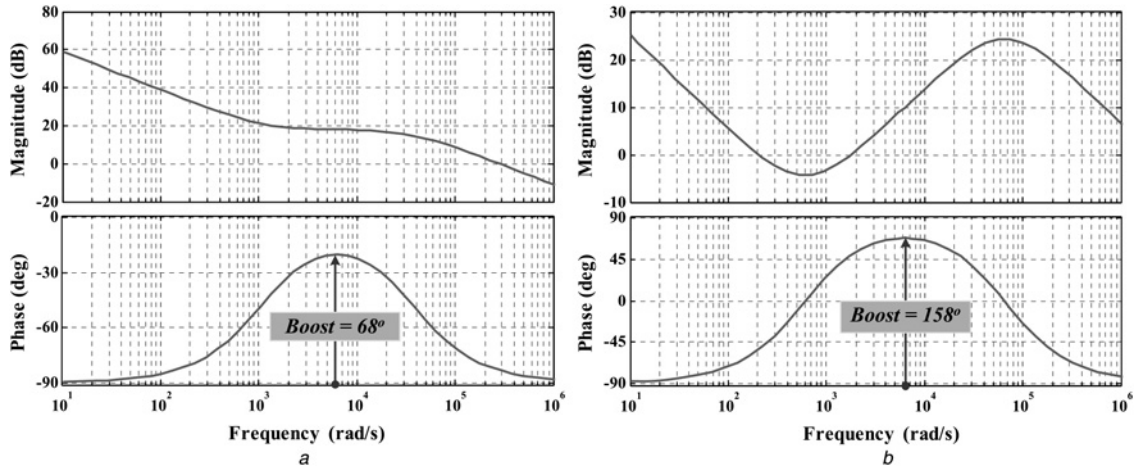

Fig. 3 *Bode diagram of*
a Type-II
b Type-III controller

68°. From (30) and (31), a pole can be placed at

$$f_{\mathrm{p}} = \tan\left(\frac{\text{phase boost}}{2} + \frac{\pi}{4}\right) f_{\mathrm{c}} = \tan\left(\frac{68^{\mathrm{o}}}{2} + 45^{\mathrm{o}}\right) \times 1000 = 5.14\ \text{kHz} \tag{33}$$

The zero is placed at

$$f_{\mathrm{z}} = \frac{f_c}{\tan(\text{phase boost}/2 + \pi/4)} = \frac{1000}{\tan(68^{\mathrm{o}}/2 + 45^{\mathrm{o}})} = 194.38\ \text{Hz} \tag{34}$$

Hence the transfer function of the designed type-II controller is given by $1000(s + 1221.3)/s(s + 32324)$.

3.2 Type-III controller design

The 'type-III' controller is lead-lead controller with a pole at origin. So, this controller provides maximum 180° phase boost with zero steady state error. Even though boost converter having non-minimum phase problem, it exhibits best closed loop performance with a type-III controller. By the proper tuning of this controller the converter may provide the fastest response (better than 'type-II' controller and PID controller) with minimal overshoots and zero steady-state error [11].

3.2.1 Mathematical approach: Type-III controller is a pair of pole-zero combination with a pole at origin. The combined transfer function of double pole-zero combination is as follows [11]

$$T_{\mathrm{c}}(s) = \frac{(1 + s/\omega_{\mathrm{z1}})(1 + s/\omega_{\mathrm{z2}})}{(s/\omega_{\mathrm{po}})(1 + s/\omega_{\mathrm{p1}})(1 + s/\omega_{\mathrm{p2}})} \tag{35}$$

Now the two zeros have been assumed at same point and similarly the two poles are also presumed same point hence the location of double pole and double zero have been considered at $\omega_{\mathrm{z1}} = \omega_{\mathrm{z2}} = \omega_{\mathrm{z1,2}}$ and $\omega_{\mathrm{p1}} = \omega_{\mathrm{p2}} = \omega_{\mathrm{p1,2}}$.

$$T_{\mathrm{c}}(s) = \frac{(1 + s/\omega_{\mathrm{z1,2}})^2}{(s/\omega_{\mathrm{po}})(1 + s/\omega_{\mathrm{p1,2}})^2} \tag{36}$$

The magnitude of the controller transfer function can be found by replacing s with $j\omega$.

$$|T_{\mathrm{c}}(j\omega)| = \frac{|1 + j\omega/\omega_{\mathrm{z1,2}}||1 + j\omega/\omega_{\mathrm{z1,2}}|}{|j\omega/\omega_{po}||1 + j\omega/\omega_{p1,2}||1 + j\omega/\omega_{p1,2}|} \tag{37}$$

The argument can be written as

$$\arg T_{\mathrm{c}}(j\omega) = 2\tan^{-1}\left(\frac{\omega}{\omega_{\mathrm{z1,2}}}\right) - 2\tan^{-1}\left(\frac{\omega}{\omega_{\mathrm{p1,2}}}\right) - \frac{\pi}{2} \tag{38}$$

The frequency response of type-III controller has been plotted in Fig. 3*b*. Here the pole-zero combinations create a phase boost of 158° at a certain frequency. In case of type-III controller the maximum 180° phase boost may be obtained by changing the poles/zeros locations. The maximum phase boost may be obtained by taking the derivate of (38) with respect to frequency f.

$$\frac{\mathrm{d}}{\mathrm{d}f}(\arg T_{\mathrm{c}}(j\omega)) = \frac{\mathrm{d}}{\mathrm{d}f}\left(2\tan^{-1}\left(\frac{f}{f_{\mathrm{z1,2}}}\right) - 2\tan^{-1}\left(\frac{f}{f_{\mathrm{p1,2}}}\right) - \frac{\pi}{2}\right) = \frac{2}{f_{\mathrm{z}}\left(f^2/f_{\mathrm{z1,2}}^2 + 1\right)} - \frac{2}{f_p\left(f^2/f_{\mathrm{p1,2}}^2 + 1\right)} = 0 \tag{39}$$

By solving f, from (39), the maximum phase boost can be obtained at the geometric means of the double zero-double pole frequencies $f_{\max} = \sqrt{f_{\mathrm{z1,2}} f_{\mathrm{p1,2}}}$. Generally this geometric mean frequency is considered as crossover frequency (f_{c}) of the controller.

3.2.2 Derivation of 'k' in type-III controller: The 'k' is defined as the ratio of the double pole frequency to the double zero frequency in type-III controller [6]. These poles-zeros combination provide maximum phase boost 180° at the crossover frequency. The relation between 'k' and the phase boost of this controller can be written as follows [10]

$$k = \left\{\tan\left(\frac{\text{phase boost}}{4} + \frac{\pi}{4}\right)\right\}^2 \tag{40}$$

Hence the pole location will be in type-III controller

$$f_{\mathrm{p1,2}} = \sqrt{k} \cdot f_{\mathrm{c}} = \tan\left(\frac{\text{phase boost}}{4} + \frac{\pi}{4}\right) f_{\mathrm{c}} \tag{41}$$

and the zero is derived from

$$f_{\mathrm{z1,2}} = \frac{f_c}{\sqrt{k}} = \frac{f_{\mathrm{c}}}{\tan(\text{phase boost}/4 + \pi/4)} \tag{42}$$

When the crossover frequency is known with the values of necessary phase boost, the exact locations of the double-pole/double-zero may be found from (41) and (42).

3.2.3 Mid-band gain adjustment for the controller: A type-III controller is simply combination of double pole/zero pair with an origin pole. The controller of (35) may be described as follows

$$T_{\mathrm{c}}(s) = \frac{s}{\omega_{\mathrm{z1}}} \frac{(\omega_{\mathrm{z1}}/s + 1)(1 + s/\omega_{\mathrm{z2}})}{s/\omega_{\mathrm{po}}(1 + s/\omega_{\mathrm{p1}})(1 + s/\omega_{\mathrm{p2}})} = G_{o\_\mathrm{III}} \frac{(\omega_{\mathrm{z1}}/s + 1)(1 + s/\omega_{\mathrm{z2}})}{(1 + s/\omega_{\mathrm{p1}})(1 + s/\omega_{\mathrm{p2}})} \tag{43}$$

In this expression, the term G_{o_III} is called the mid-band gain and G_{o_III} is equal to $\omega_{\mathrm{po}}/\omega_{\mathrm{z1}}$. The location of ω_{z1} should be fixed by the amount of required phase boost and the location of ω_{po} depends upon the required gain/attenuation at crossover frequency.

Now

$$G_{o\_\mathrm{III}} = G_{\mathrm{III}} \frac{\left[\sqrt{1 + (\omega_{\mathrm{c}}/\omega_{\mathrm{p1}})^2}\sqrt{1 + (\omega_{\mathrm{c}}/\omega_{\mathrm{p2}})^2}\right]}{\left[\sqrt{1 + (\omega_{\mathrm{z1}}/\omega_{\mathrm{c}})^2}\sqrt{1 + (\omega_{\mathrm{c}}/\omega_{\mathrm{z2}})^2}\right]} \tag{44}$$

IET Power Electron., 2016, Vol. 9, Iss. 5, pp. 938–950

G_{III} is an assumed gain at crossover frequency f_c.

$$\omega_{po} = G_{III} \cdot \omega_{z1} \frac{\left[\sqrt{1+\left(\omega_c/\omega_{p1}\right)^2}\sqrt{1+\left(\omega_c/\omega_{p2}\right)^2}\right]}{\left[\sqrt{1+\left(\omega_{z1}/\omega_c\right)^2}\sqrt{1+\left(\omega_c/\omega_{z2}\right)^2}\right]} \quad (45)$$

If double coincident poles/zeros pair has been considered, the formula becomes

$$\omega_{po} = G_{III}.\omega_{z1,2} \frac{\left[\omega_{p1,2}^2 + \omega_c^2\right]}{\left[\omega_{p1,2}^2\sqrt{\left(\omega_{z1,2}/\omega_c\right)^2+1}\sqrt{\left(\omega_c/\omega_{z1,2}\right)^2+1}\right]} \quad (46)$$

As $\omega_{z1,2}$ is fixed by the amount of required phase boost, ω_{po} will be placed depending on the desired gain/attenuation at crossover frequency.

3.2.4 Design example with a type III: Let us assume a power supply that has a gain deficit of −10 dB at a 1 kHz selected crossover frequency. The necessary phase boost is 158°. From (41) and (42), the position of the double pole will be as follows

$$\begin{aligned} f_{p1,2} &= \tan\left(\frac{\text{phase boost}}{4} + \frac{\pi}{4}\right) f_c \\ &= \tan\left(\frac{158^\circ}{4} + 45^\circ\right) \times 1000 = 10.38\,\text{kHz} \end{aligned} \quad (47)$$

The double zero is placed at

$$\begin{aligned} f_{z1,2} &= \frac{f_c}{\tan(\text{phase boost}/4 + \pi/4)} \\ &= \frac{1000}{\tan(158^\circ/4 + 45^\circ)} = 96.28\,\text{Hz} \end{aligned} \quad (48)$$

The gain G at 1 kHz has chosen −10 dB. Hence the position of the 0-dB crossover pole at

$$\begin{aligned} f_{po} &= G.f_{z1,2} \frac{\left(f_{p1,2}^2 + f_c^2\right)}{f_{p1,2}^2\sqrt{\left(f_{z1,2}/f_c\right)^2+1}\sqrt{\left(f_c/f_{z1,2}\right)^2+1}} \\ &= \frac{10^{-10/-20} \times 96.28 \times 1000^2 \times \left(10.38^2+1\right)}{10.38^2 \times 1000^2 \times \sqrt{1+\left(96.28/1000\right)^2}\sqrt{1+\left(1000/96.28\right)^2}} \\ &= 29.30\,\text{Hz} \end{aligned} \quad (49)$$

Hence the transfer function of the designed type-III controller is given by $3.003 \times 10^6(s+605)^2/s(s^2+1.31 \times 10^5 s + 4.26 \times 10^9)$.

4 Particle swarm optimisation

4.1 Overview

The PSO [12–15] is an evolutionary algorithm (technique) that can optimise the linear or non-linear, continues or discrete, constrained or unconstrained, non-differentiable functions by iteratively trying to improve the solutions for different parameter values [23]. The PSO algorithm is based on the behaviour of a colony of living things, such as school of fish, flock of birds, or swarm of insects. The insects, fishes, animals, especially birds etc., always travel in a group without crashing each other from their group members by adjusting their positions and velocities from using their group information.

4.2 Computational implementation of PSO

Fitness function: The fitness function with typical performance criteria is the first step for designing the PSO based optimised type-II/III controllers with desired specifications and constraints under input step signal. Some important output specifications in the time domain are overshoot, rise time, settling time, and steady-state error. Generally, there are four kinds of performance criteria [5], such as the integral absolute error, the integral of squared error (ISE), the integral of time weighted squared error, and the integral of time weighted absolute error (ITAE). Since ITAE performance criterion provides fastest response with small overshoot for a class of optimisation techniques, hence $\text{ITAE}_{\text{fitness}}$ is chosen as a fitness function in this simulation study and is represented by

$$\text{ITAE}_{\text{fitness}} = \int_0^\tau t|e(t)|\text{d}t \quad (50)$$

where, the upper limit τ is chosen as steady-state value.

A concise idea about the PSO algorithm has been described here for a U-dimensional search space with n_u particles. Consider the ith particle and the particle can be expressed by a position vector: $S_i = (s_{i1}, s_{i2}, \ldots, s_{iU})$ and a velocity vector: $V_i = (v_{i1}, v_{i2}, \ldots, v_{iU})$.

The historical best value of position vector for the ith particle can be described as $pbest_i = (p_{i1}, p_{i2}, \ldots, p_{iU})$, and group best can be expressed as $gbest = (p_{g1}, p_{g2}, \ldots, p_{gU})$.

The maximum and minimum velocity vectors are mentioned as V_{max}, and V_{min}.

where $V_{max} = (v_{max1}, v_{max2}, \ldots, v_{maxU})$ and $V_{min} = (v_{min1}, v_{min2}, \ldots, v_{minU})$.

The positive constants c_1 and c_2 are the individual (cognitive) and group (social) learning rates, respectively, and r_1 and r_2 are uniformly distributed random numbers in the range [0, 1]. The parameters c_1 and c_2 denote the relative importance of the memory (position) of the particle itself to the memory (position) of the swarm. The values of c_1 and c_2 are usually assumed to be 2 so that c_1r_1 and c_2r_2 ensure that the particles would overfly the target about half the time. The inertia weight constant w has to be chosen carefully for obtaining the optimum result with fast convergence and $þ$ denotes the iteration number.

The basic steps of the PSO algorithm are as follows:

Step 1: Initialise the particles of n_u population.
Step 2: Compute the error fitness value for the current position S_i of each particle.
Step 3: Each particle can remember its best position (*pbest*) which is known as cognitive information and that would be updated with each iteration.
Step 4: Each particle can also remember the best position the swarm has ever attained (*gbest*) and is called social information and the value would be updated in each iteration.
Step 5: Velocity and position vector of each particle are modified according to (51) and (52), respectively.

$$\begin{aligned} V_i^{(þ+1)} &= wV_i^{(þ)} + c_1r_1\left[p\text{best}_i^{(þ)} - S_i^{(þ)}\right] \\ &\quad + c_2r_2\left[g\text{best}^{(þ)} - S_i^{(þ)}\right] \end{aligned} \quad (51)$$

$$S_i^{(þ+1)} = S_i^{(þ)} + V_i^{(þ+1)} \quad (52)$$

Step 6: The iteration stops when maximum number of cycles is reached and the desired solution can be found for the corresponding particle. Otherwise the iterative process repeats.

4.3 Optimisation specifications

The parameters of the type-II and type-III controllers are to be optimised using PSO based optimisation technique. There are

actually four parameters for type-II controllers, but for optimisation three parameters are considered, namely DC gain, one zero and one pole. Similarly for type-III controller for optimisation one DC gain, one pair of zeros and one pair of poles have been considered. In both the cases the pole at origin has not been considered because of fixed location. The flowchart of the optimisation process is given in Fig. 4. The routine for PSO has been written in MATLAB (version R2011a). A swarm of 50 particles characterised by three parameters has been initialised. The controller parameters have been initialised and the values are constrained within a range. Optimised result has been obtained after 100 iterations beyond which significant improvement has not been observed. The values for the PSO parameters are given in Table 2.

Table 2 Parameters of PSO method

Sl. No.	Parameter	Value
1	inertia weight constant (w)	0.73
2	cognitive constant (c_1)	1.44495
3	group constant (c_2)	1.44495
4	number of particles (n_u)	50
5	number of iteration (b)	100

5 Gravitational search algorithm

5.1 Overview

GSA, a new optimisation algorithm, is based on the law of gravity (Rashedi *et al.*, 2009) [16, 17]. In this computing technique, the particles are considered as objects and their performance is measured by their masses. All these objects attract each other by the gravity force, and this force causes a global movement of all objects. Hence, masses cooperate using a direct form of communication, through gravitational force. The heavy masses (which correspond to good solutions) move more slowly than lighter ones. This guarantees the exploitation step of the algorithm. Three kinds of masses are defined in theoretical physics: (i) Active gravitational mass (M_a) is a measure of the strength of the gravitational field due to a particular objet, (ii) Passive gravitational mass (M_p) is a measure of the strength of an object's interaction with the gravitational field, and (iii) Inertial mass (M_i) is a measure of an object's resistance to changing its state of motion when a force is applied [16, 25]. An object with small inertial mass changes it rapidly.

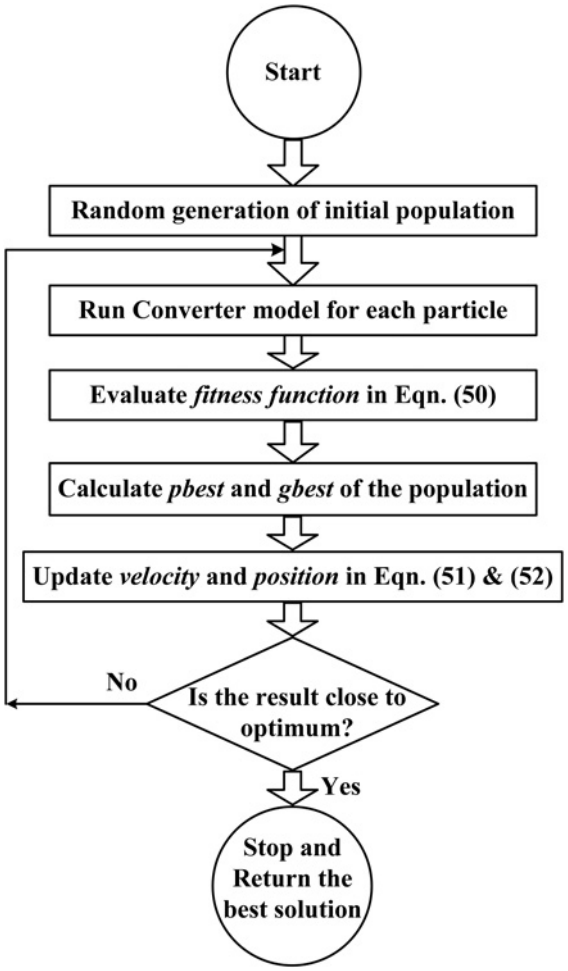

Fig. 4 *Flowchart of the optimisation process*

In GSA, each mass (particle) has four specifications: position, internal mass, active gravitational mass, and passive gravitational mass. The position of mass corresponds to a solution of problem, and its gravitational and inertial masses are determined using a fitness function (refer (50)). In other words, each mass presents a solution, and the algorithm is navigated by properly adjusting the gravitational and inertia masses.

The GSA could be considered as an isolated system of masses. It is like a small artificial world of masses obeying the Newtonian laws of gravitation and motion. More precisely, masses obey the following laws: [16, 25].

Law of gravity: Every particle in the universe attracts every other particle and the gravitational force between two particles is directly to the product of their masses and inversely proportional to the square of the distance (D) between them. Rashedi *et al.* [16] used D instead of D^2 because D offered better results than D^2 in all their experimental cases with benchmark functions. Using single exponent instead of double exponent for D causes the departure of the present GSA from exact Newtonian Law of gravitation.

Law of motion: The current velocity of any mass is equal to the sum of the fraction of its previous velocity and the variation in the velocity. Variation in velocity or acceleration of any mass is equal to the force acted on the system divided by the mass of inertia.

5.2 Computational implementation of GSA

Let, the position of the qth particle (masses) among the n_p total number of particle vectors (population) can be explained by

$$Z_q = (Z_q^1, Z_q^2, Z_q^3, \ldots, Z_q^d, \ldots, Z_q^n) \text{ for } q = 1, 2, \ldots, n_p \quad (53)$$

where Z_q^d represents the position of qth particle vector in the dth dimension and n is total number of dimension.

In our study each particle vector of the population n_p denotes three parameters or dimension for type-II controller (Z_q^1 = controller gain, Z_q^2 = zero location, and Z_q^3 = pole location) and five parameters or dimension for type-III controller (Z_q^1 = controller gain, Z_q^2 = 1st zero location, Z_q^3 = 2nd zero location, Z_q^4 = 1st pole location, and Z_q^5 = 2nd pole location).

At time 't' a gravitational force is acting on particle 'q' from particle 'j' can be written as (54)

$$F_{qj}^d(t) = G(t)\frac{M_{pq}(t) \times M_{aj}(t)}{D_{qj}(t) + \varepsilon}\left(Z_j^d(t) - Z_q^d(t)\right) \quad (54)$$

where, $G(t)$ is gravitational constant at time t, M_{aj} is the active mass and M_{pq} is the passive mass related to the particles q and j. ε is a small constant, and $D_{qj}(t)$ is the Euclidian distance between two particles q & j.

$$D_{qj}(t) = \left\| Z_q(t) Z_j(t) \right\|_2 \quad (55)$$

In other words, the gravitational constant $G(t)$ is a function of the initial value (G_0) and iteration time t

$$G(t) = G_0 e^{-\alpha(t/t_{\max})} \tag{56}$$

where $t_{\max}$ is the maximum iteration. α is positive constant.

In this algorithm, it is assumed that the total force on particle q, F_q^d is the sum of randomly weighted the force components F_{qj} from other particles at time t in a dimension d

$$F_q^d(t) = \sum_{j=1, j\neq q}^{n_p} rand_j F_{qj}^d(t) \tag{57}$$

where $rand_j$ is a random number in the interval [0, 1].

The technique is used to perform a good compromise between exploration and exploitation is to decrease the number of agents with lapse of iteration number in (57). Therefore, only a set of agents with higher masses apply their forces to others but it may because the exploration power and increase the exploration capability. To control exploration and exploitation, only *Kbest* agents will attract each other. *Kbest* is the function of iteration cycle number. *Kbest* is computed in such a manner that it decreases linearly with time and at last iteration the value of *Kbest* becomes 2% of the initial number of agents. Now, the modified force equation becomes

$$F_q^d(t) = \sum_{j=Kbest, j\neq q}^{n_p} rand_j F_{qj}^d(t) \tag{58}$$

According to the law of motion, the acceleration of qth particle at dth dimension

$$a_q^d(t) = \frac{F_q^d(t)}{M_{qq}(t)} \tag{59}$$

where M_{qq} is the inertial mass of qth particle.

The velocity ($\hat{h}$) and position updating formulae are given below

$$\hat{h}_q^d(t+1) = rand_q \times \hat{h}_q^d(t) + a_q^d(t) \tag{60}$$

$$Z_q^d(t+1) = Z_q^d(t) + \hat{h}_q^d(t+1) \tag{61}$$

where $rand_q$ is a uniform random variable in the interval [0,1].

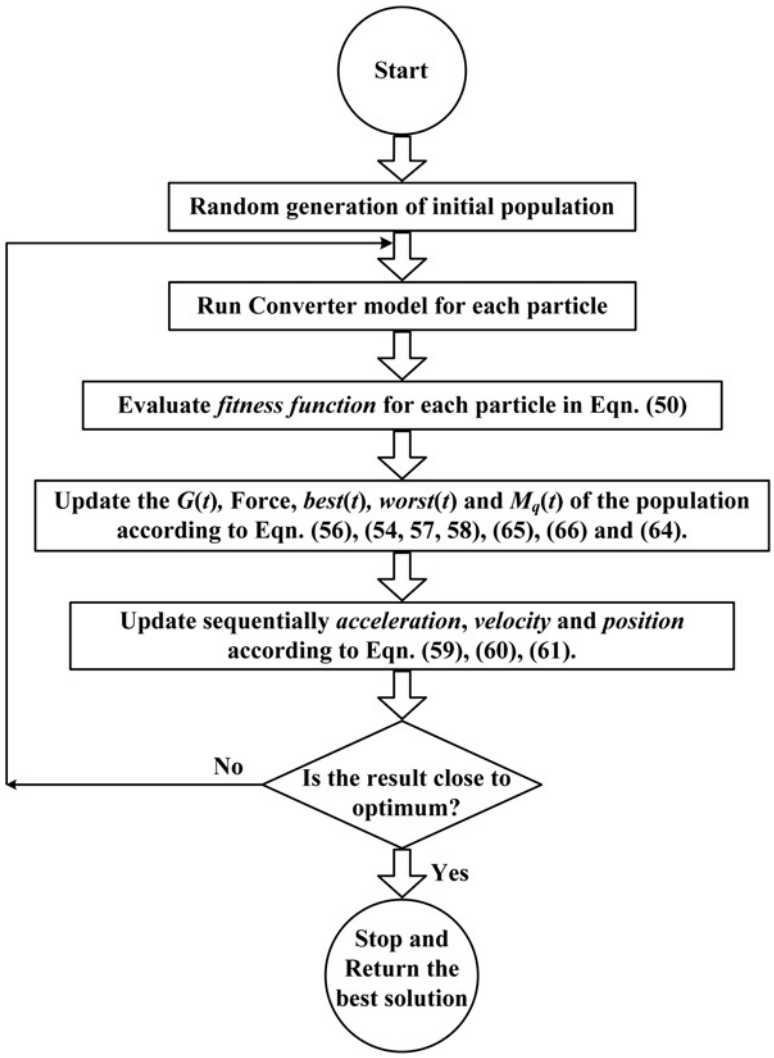

Fig. 5 *Flowchart of the GSA optimisation process*

Table 3 Parameters of GSA method

Sl. No.	Parameter	Value
1	constant (G_0)	3
2	constant (α)	2
3	number of particles (n_p)	50
4	number of iteration (t_{max})	100

The gravitational and inertia masses are simply calculated by using (63) and (64).

$$M_{aq} = M_{pq} = M_{qq} = M_q, \quad \text{where } q = 1, 2, \ldots, n_p. \tag{62}$$

$$\hat{m}_q(t) = \frac{\text{fit}_q(t) - \text{worst}(t)}{\text{best}(t) - \text{worst}(t)} \tag{63}$$

$$M_q(t) = \frac{\hat{m}_q(t)}{\sum_{j=1}^{n_p} \hat{m}_q(t)} \tag{64}$$

where $\text{fit}_q(t)$ represent the fitness value of the particle q at time t, and, $\text{worst}(t)$ and $\text{best}(t)$ are defined as follows

$$\text{best}(t) = \min_{j \in \{1,2\ldots,n_p\}} \text{fit}_j(t) \tag{65}$$

$$\text{worst}(t) = \max_{j \in \{1,2\ldots,n_p\}} \text{fit}_j(t) \tag{66}$$

The flow chart of GSA has been given in Fig. 5.

5.3 Optimisation specifications

The parameters of the type-II/III controllers are to be optimised using GSA based optimisation technique. For type-II controllers, three parameters (controller gain, one zero and one pole) and type-III controller, five parameters (controller gain, one pair of zeros and one pair of poles) have been optimised. In both the cases the pole at origin has not been considered because of fixed location. The flowchart of the optimisation process is given in Fig. 5. The routine for GSA has been written in MATLAB (version R2011a). The values for the GSA parameters are given in Table 3.

6 Simulation results and discussion

Extensive simulation has been carried out to determine the parameters of type-II/type-III controllers and PID controller by using classical and two different optimisation techniques (PSO and GSA) so that the closed loop performance of the converter becomes satisfactory. The dynamic performances in terms of step and frequency response of the DC–DC boost converter with type-II/type-III controllers and PID controller have been reported in Figs. 6a and *b* and corresponding specifications are given in Table 4. It is clear that optimised type-III controllers provide best dynamic response than other controllers. The time response with optimised type-III controllers shows very fast response with no overshoot and zero steady-state error. It is to be mentioned here that the '*k*-factor' approach is a standard method for design of Type controllers and in the present case it worked well for the closed loop boost converter. However, keeping in view the demand for very fast response of power supply, the controller

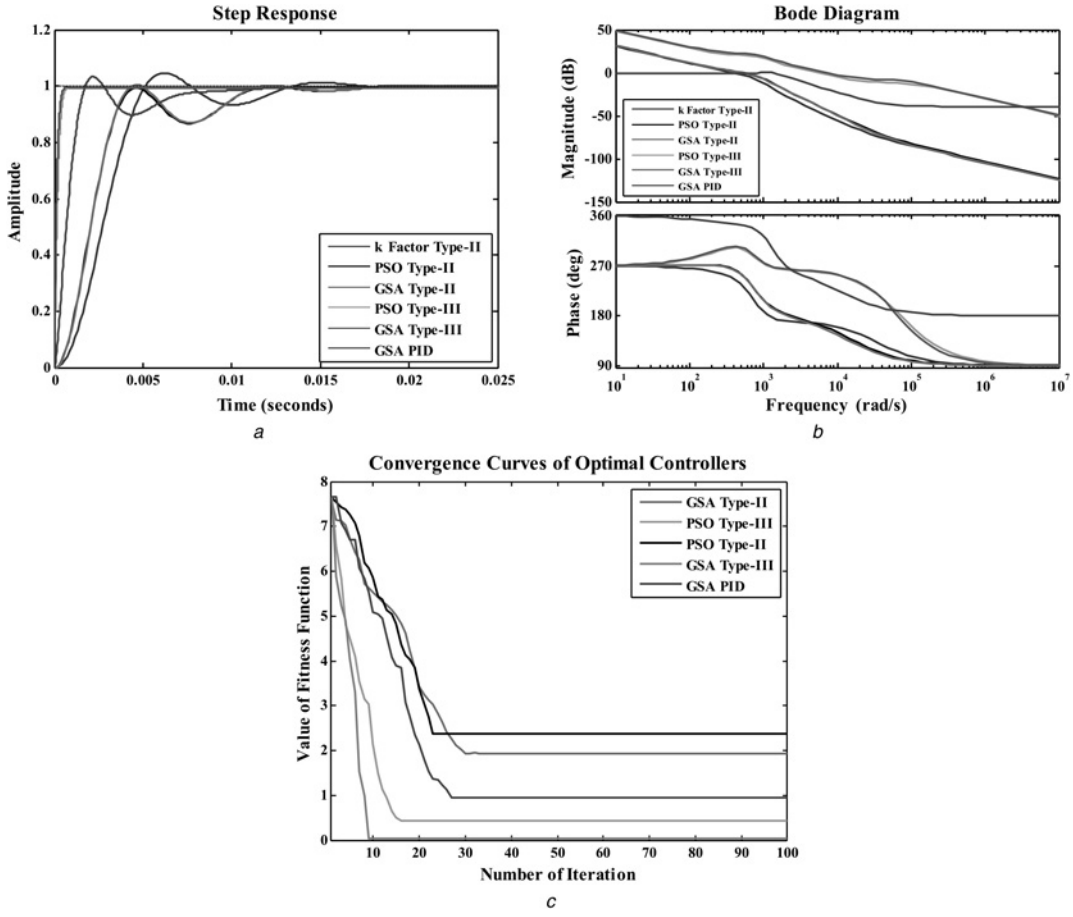

Fig. 6 *Closed loop dynamic performances of the DC–DC boost converter with type-II/type-III controllers and PID controller*

a Step responses
b Bode diagram
c Convergence curves of fitness function ($\text{ITAE}_{\text{fitness}}$) for optimised type-II/III and PID controller

Table 4 Comparative study of closed-loop performances

Parameter	Type-II, *k*-factor approach	Type-II, PSO	Type-II, GSA	PID controller, GSA	Type-III, PSO	Type-III, GSA
maximum overshoot (M_p)	4.52%	0%	0%	3.31%	0.047%	0%
rise time (t_r)	0.0050 s	0.0047 s	0.0043 s	0.00118 s	0.000273 s	0.000245 s
settling time (t_s)	0.0125 s	0.0108 s	0.0107 s	0.00852 s	0.000465 s	0.000437 s
steady-state error (E_{ss})	0	0	0	0	0	0
phase margin (PM)	67.4°	69.7°	70.9°	60.8°	78°	79.3°
gain crossover frequency (GCF)	391 rad/sec	567 rad/sec	544 rad/sec	1350 rad/sec	6450 rad/sec	7260 rad/sec
phase crossover frequency (PCF)	1210 rad/sec	2380 rad/sec	2380 rad/sec	Inf	72,900 rad/sec	66,500 rad/sec
controller gain (G_o)	1000	1243.1556	1014.0845	1.9145	6.57×10^6	6.08×10^6
controller transfer function (T_c)	$\frac{1000(s+1221.3)}{s(s+32324)}$	$\frac{1243.1556(s+540.9)}{s(s+16540)}$	$\frac{1014.0845(s+555.56)}{s(s+14084.50704)}$	$\frac{1.9145(s+1418.7)(s+417.11)}{s(s+11486)}$	$\frac{6.57\times10^6(s+524.7)^2}{s(s+7.308\times10^4)^2}$	$\frac{6.08\times10^6(s+500.1905)^2}{s(s^2+1.144\times10^5 s+4.44\times10^9)}$
closed-loop stability	stable	stable	stable	stable	stable	stable

parameters (both PID and Type controllers) are further optimised by using PSO and GSA method. In the frequency domain analysis it is observed that GSA based type-III controller generates maximum phase margin (79.3°) and highest gain crossover frequency (7260 rad/s). Due to have an edge in performance, GSA based technique is considered for practical application. Fig. 6*c* shows the plot of minimum values of the fitness function ($ITAE_{fitness}$) against number of iterations for type-II and type-III controller. It is seen that the GSA based type-III controller produces the least fitness function ($ITAE_{fitness}$) value than other optimised type-II/type-III and PID controllers. From Fig. 6 and Table 4, it is clear that the performance of optimised type-III controller is better than optimised PID controller for the proposed boost converter.

7 Stability analysis of closed loop converter with GSA based optimised type-III controller

The proposed GSA base optimised type-III controller has been chosen for practical implementation. From the characteristic ((67)), it has been observed that the closed-loop roots are present in the left half of '*s*' plane which confirms overall system stability. The closed loop root locus and bode plot of the boost converter (Fig. 7) cascaded with proposed GSA based type-III controller also verifies that the closed loop system is conditionally stable.

The characteristic equation is

$$1 + G(s)H(s) = 0$$

$$\text{or, } 1 + T_{P\_\text{Boost}}(s) \times T_{\text{c\_GSA\_Type}-III}(s) \times 1 = 0$$

$$\text{or, } 1 + \left(\frac{-0.005696s^2 - 0.02559s + 4.983 \times 10^6}{s^2 + 825.3s + 542410}\right) \times \left(\frac{6.08 \times 10^6 (s + 500.1905)^2}{s\left(s^2 + 1.144 \times 10^5 s + 4.44 \times 10^9\right)}\right) = 0 \quad (67)$$

The roots of (67) are $-360.18, -720.08, -7551.75, -35980.81 + j50797.47, -35980.81 - j50797.47$. All the closed-loop roots present LHP of the *s*-domain, hence the system is stable.

8 Experimental results

The closed loop boost converter has been implemented practically with the designed controllers utilising dSPACE based real time system. The overall experimental setup of the system is shown in Fig. 8. From the simulation results (Fig. 6), it is clear that for the given converter GSA based optimised type-III controller exhibits best performance and '*k*-factor' based classical type-II controller produces relatively worst result while comparing the closed loop performances with different control algorithms. Since optimised PID controller is reported [18–35] for controlling the DC–DC converters, in the implementation part, GSA based PID controller is also used with aforesaid two controllers ('*k*-factor' based classical type-II controller and GSA based optimised type-III controller) for the closed-loop control of the proposed boost converter. Fig. 9 shows the dynamic responses of output voltage, coil-current and coil-voltage for the case of boost converter with (i) GSA based optimised type-III, (ii) GSA based PID controller and (iii) classical type-II controller with positive step change in load voltage, respectively. It is clear that GSA based proposed type-III controller exhibits the fastest response without producing any overshoot and worst result in terms of sluggishness and overshooting is noted in case of '*k*-factor' based classical type-II. The coil-current and coil-voltage dynamics also been observed in Fig. 9. A current probe has been used to measure the coil current (with a scale of 100 mV = 1A). During '*switch on*' condition the coil voltage is the input voltage and '*switch off*' condition the coil voltage equals to the difference between output & input voltage of the converter. As expected, there is overshooting in the output

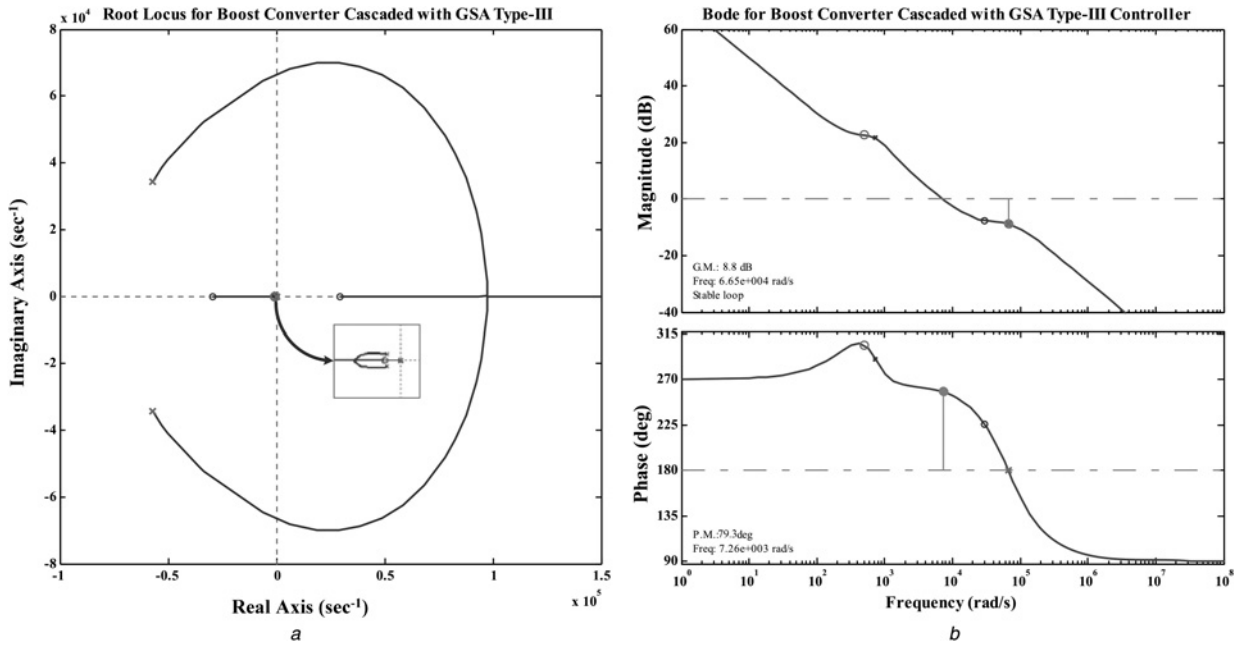

Fig. 7 *Closed loop root locus and bode plot of the boost converter with proposed GSA based type-III controller*

a Root locus
b Bode-plot of boost converter cascaded

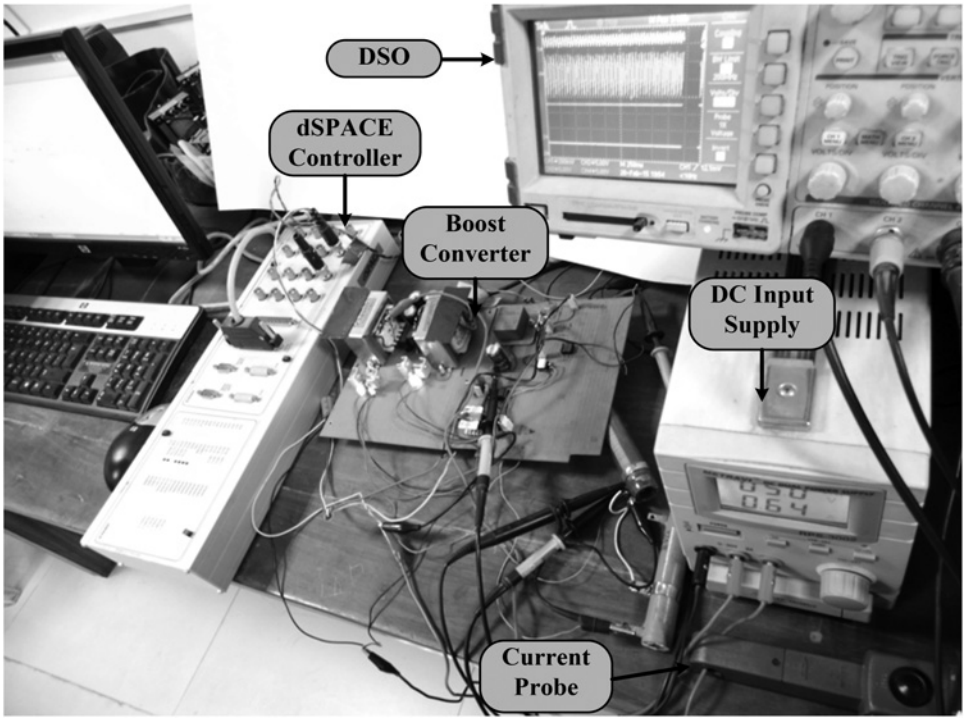

Fig. 8 *Overall experimental setup*

voltage response due to positive step change in load in case of GSA based PID controller and '*k-factor*' based classical type-II controller approach (Figs. 9*b* and *c*).

9 Conclusion

This paper describes design and implementations of type controllers by using '*k*-factor' approach and optimisation techniques (GSA and PSO) for obtaining better stability and performance for a DC–DC switched mode boost converter. The closed loop performances and the comparative analysis for classical and optimised PID, type-II/III controllers for the boost converter have been studied both in simulation and experimentation. It may be concluded that the optimised type-III controllers exhibit the best closed-loop performance, highest system bandwidth and largest margin of stability. Hence optimised type-III controllers may be used for the design and implementation of SMPS utilising boost converter to

IET Power Electron., 2016, Vol. 9, Iss. 5, pp. 938–950

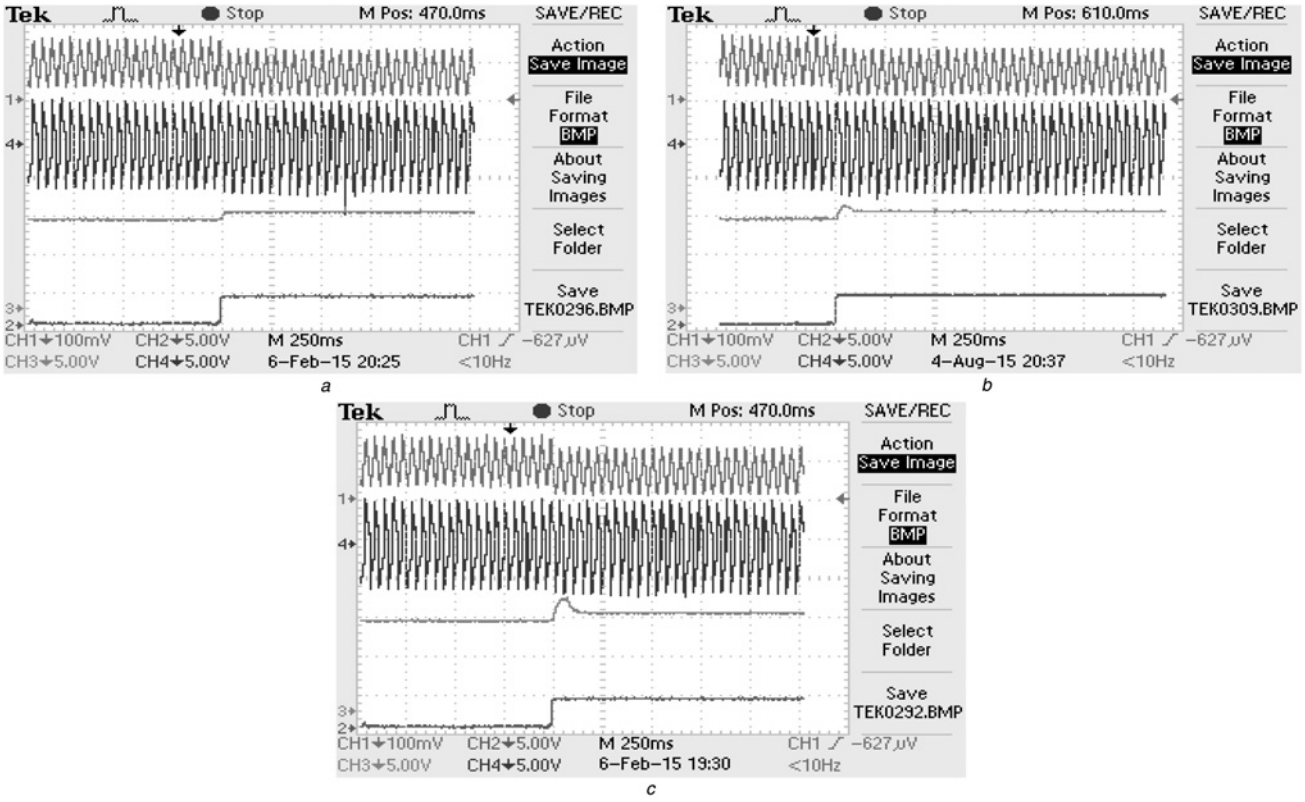

Fig. 9 *Transient response with positive step load disturbance with*

a GSA type-III controller
b GSA PID controller
c '*k*-factor' type-II controller. [Where Ch1: coil current, Ch2: load disturbance, Ch3: load voltage and Ch4: coil voltage]

improve the overall closed loop stability and performance. The proposed control algorithm though applied for lower rated converter, but it may be applicable for higher rating also.

10 References

1 Mohan, N., Undeland, T.M., Robbins, W.P.: 'Power electronics: converters, applications, and design' (John Wiley & Sons, 2007)
2 Erickson, R.W., Maksimovic, D.: 'Fundamentals of power electronics' (Springer, 2007)
3 Veerachary, M.: 'Control of power electronic systems – digital solutions' (2012)
4 Ogata, K.: 'Modern control engineering' (Pearson Education, India, 2010)
5 Dorf, R.C., Bishop, R.H.: 'Modern control systems' (Pearson, 2011)
6 Venable, H.D.: 'The k-factor: a new mathematical tool for stability analysis and synthesis'. Proc. of Powercon 10, CA, 1983
7 Reatti, A., Kazimierczuk, M.K.: 'Small-signal model of PWM converters for discontinuous conduction mode and its application for boost converter', *IEEE Trans. Circuits Syst. I: Fundam. Theory Appl.*, 2003, **50**, (1), pp. 65–73
8 Bryant, B., Kazimierczuk, M.K.: 'Voltage loop of boost PWM DC-DC converters with peak current-mode control', *IEEE Trans. Circuits Syst. I: Fundam. Theory Appl.*, 2006, **53**, (1), pp. 99–105
9 Lee, S.W.: 'Practical feedback loop analysis for voltage-mode boost converter' (SLVA633, Texas Instruments, 2014)
10 Ghosh, A., Banerjee, S.: 'Design of type-III controller for DC-DC switch-mode boost converter'. IEEE sixth Power India Int. Conf. (PIICON-2014), Delhi Technological University, New Delhi, India, 5–7 December 2014, pp. 1–6, (doi: 10.1109/34084POWERI.2014.7117679)
11 Ghosh, A., Banerjee, S.: 'Design and implementation of type-II compensator in DC-DC switch-mode step-up power supply'. IEEE Third Int. Conf. on Computer, Communication, Control and Information Technology (C3IT-2015), Academy of Technology, Hooghly, India, 7–8 February 2015, pp. 1–5 (doi: 10.1109/C3IT.2015.7060164)
12 Eberhart, R.C., Kennedy, J.: 'A new optimizer using particle swarm theory'. sixth Int. Symp. on Micro Machine and Human Science, 1995, vol. 1, pp. 39–43
13 AlRashidi, M.R., El-Hawary, M.E.: 'A survey of particle swarm optimization applications in electric power systems', *IEEE Trans. Evol. Comput.*, 2009, **13**, (4), pp. 913–918
14 Kennedy, J.: 'Particle swarm optimization', in Sammut, C., Webb, G.I. (eds): 'Encyclopaedia of Machine Learning', (Springer, 2010), pp. 760–766
15 Clerc, M.: 'Particle swarm optimization' (John Wiley & Sons, 2010)
16 Rashedi, E., Nezamabadi-Pour, H., Saryazdi, S.: 'GSA: a gravitational search algorithm', *Inf. Sci.*, 2009, **179**, (13), pp. 2232–2248
17 Sabri, N.M., Puteh, M., Mahmood, M.R.: 'A review of gravitational search algorithm', *Int. J. Adv. Soft Comput. Appl*, 2013, **5**, (3), pp. 1–39
18 Beccuti, A.G., Papafotiou, G., Morari, M.: 'Optimal control of the boost DC-DC converter'. IEEE 44th Conf. on Decision and Control and European Control Conf. (CDC-ECC'05), 2005, pp. 4457–4462
19 Emami, S.A., Poudeh, M.B., Eshtehardiha, S.: 'Particle Swarm Optimization for improved performance of PID controller on Buck converter'. IEEE Int. Conf. on Mechatronics and Automation (ICMA 2008), 2008, pp. 520–524
20 Liu, C.H., Hsu, Y.Y.: 'Design of a self-tuning PI controller for a STATCOM using particle swarm optimization', *IEEE Trans. Ind. Electron.*, 2010, **57**, (2), pp. 702–715
21 Altinoz, O.T., Erdem, H.: 'Evaluation function comparison of particle swarm optimization for buck converter'. IEEE Int. Symp. on Power Electronics Electrical Drives Automation and Motion (SPEEDAM), 2010, pp. 798–802
22 Jalilvand, A., Kimiyaghalam, A., Ashouri, A., *et al.*: 'Optimal tuning of PID controller parameters on a DC motor based on advanced particle swarm optimization algorithm', *Int. J. Tech. Phys. Probl. Eng. Optim.*, 2011, **3**, (4), pp. 10–12
23 Khare, A., Rangnekar, S.: 'A review of particle swarm optimization and its applications in solar photovoltaic system', *Appl. Soft Comput.*, 2013, **13**, (5), pp. 2997–3006
24 Duman, S., Maden, D., Guvenc, U.: 'Determination of the PID controller parameters for speed and position control of DC motor using gravitational search algorithm'. IEEE Seventh Int. Conf. on Electrical and Electronics Engineering (ELECO), 2011, pp. I–225
25 Sarkar, M.K., Banerjee, S., Saha, T.K., *et al.*: 'Implementation of GSA based optimal lead-lead controller for stabilization and performance enhancement of a DC electromagnetic levitation system', *J. Control Eng. Appl. Inf.*, 2013, **15**, (3), pp. 11–20
26 Zobaa, A.F., Lecci, A.: 'Particle swarm optimisation of resonant controller parameters for power converters', *IET Power Electron.*, 2011, **4**, (2), pp. 235–241
27 Sundareswaran, K., Sreedevi, V.T.: 'Boost converter controller design using queen-bee-assisted GA', *IEEE Trans. Ind. Electron.*, 2009, **56**, (3), pp. 778–783
28 Davoudi, A., Kong, N., Behjati, H., *et al.*: 'Automated system identification and controller tuning for digitally controlled dc–dc converters', *IET Power Electron.*, 2012, **5**, (6), pp. 765–772 (doi: 10.1049/iet-pel.2011.0085)
29 Lefranc, P., Jannot, X., Dessante, P. : 'Virtual prototyping and pre-sizing methodology for buck DC-DC converters using genetic algorithms', *IET Power Electron.*, 2012, **5**, (1), pp. 41–52 (doi: 10.1049/iet-pel.2010.0284)
30 Wang, Q., An, Z., Zheng, Y., *et al.*: 'Parameter extraction of conducted electromagnetic interference prediction model and optimisation design for a DC–DC converter system', *IET Power Electron.*, 2013, **6**, (7), pp. 1449–1461 (doi: 10.1049/iet-pel.2013.0001)

31 Eskandari, B., Bina, M.T., Golkar, M.A.: 'New concept on sinusoidal modulation for three-phase DC/AC converters: analysis and experiments', *IET Power Electron.*, 2013, **7**, (2), pp. 357–365 (doi: 10.1049/iet-pel.2012.0707)

32 El Khateb, A., Rahim, N.A., Selvaraj, J., *et al.*: 'Maximum power point tracking of single-ended primary-inductor converter employing a novel optimisation technique for proportional-integral-derivative controller', *IET Power Electron.*, 2013, **6**, (6), pp. 1111–1121 (doi: 10.1049/iet-pel.2012.0416)

33 Sundareswaran, K., Devi, V., Sankar, S., *et al.*: 'Feedback controller design for a boost converter through evolutionary algorithms', *IET Power Electron.*, 2014, **7**, (4), pp. 903–913

34 Behjati, H., Davoudi, A.: 'Reference-change response assignment for pulse-width-modulated dc-dc converters', *IET Power Electron.*, 2014, **7**, (6), pp. 1414–1423

35 Evzelman, M., Peretz, M.M.: 'Optimal design of a class-E resonant driver', *IET Power Electron.*, 2015, **8**, (8), pp. 1552–1557 (doi: 10.1049/iet-pel.2014.0397)

36 Krein, P.T., Bentsman, J., Bass, R.M., *et al.*: 'On the use of averaging for the analysis of power electronic systems', *IEEE Trans. Power Electron.*, 1990, **5**, (2), pp. 182–190

37 Gezgin, C., Heck, B.S., Bass, R.M.: 'Simultaneous design of power stage and controller for switching power supplies', *IEEE Trans. Power Electron.*, 1997, **12**, (3), pp. 558–566

38 Wu, W.C., Bass, R.M., Yeargan, J.R.: 'Eliminating the effects of the right-half plane zero in fixed frequency boost converters'. IEEE 29th Power Electronics Specialists Conf. (PESC 98), 1998, vol. 1, pp. 362–366

39 Salimi, M., Soltani, J., Markadeh, G.A., *et al.*: 'Indirect output voltage regulation of dc-dc buck/boost converter operating in continuous and discontinuous conduction modes using adaptive backstepping approach', *IET Power Electron.*, 2013, **6**, (4), pp. 732–741 (doi: 10.1049/iet-pel.2012.0198)

40 Salimi, M., Soltani, J., Zakipour, A., *et al.*: 'Hyper-plane sliding mode control of the DC–DC buck/boost converter in continuous and discontinuous conduction modes of operation', *IET Power Electron.*, 2015, **8**, (8), pp. 1473–1482 (doi: 10.1049/iet-pel.2014.0578)

41 Ma, H., Liu, Q., Wang, Y.: 'Discrete pulse frequency modulation control with sliding-mode implementation on LLC resonant DC/DC converter via input–output linearisation', *IET Power Electron.*, 2014, **7**, (5), pp. 1033–1043 (doi: 10.1049/iet-pel.2013.0399)

42 Zhou, L., Liu, S., Lu, W., *et al.*: 'Quasi-steady-state large-signal modelling of DC–DC switching converter: justification and application for varying operating conditions', *IET Power Electron.*, 2014, **7**, (10), pp. 2455–2464

43 Alonge, F., D'Ippolito, F., Raimondi, F.M., *et al.*: 'Nonlinear modeling of DC/DC converters using the Hammerstein's approach', *IEEE Trans. Power Electron.*, 2007, **22**, (4), pp. 1210–1221